frontiers | Frontiers in Earth Science

TYPE Original Research
PUBLISHED 30 April 2025
DOI 10.3389/feart.2025.1583402

OPEN ACCESS

EDITED BY
Tongming Qu,
Hong Kong University of Science and Technology, Hong Kong SAR, China

REVIEWED BY
Dengguo Li,
Jiaxing University, China
Xiong Wang,
Shanghai Jiao Tong University, China

*CORRESPONDENCE
Zeliang Li,
525065355@qq.com

RECEIVED 25 February 2025
ACCEPTED 10 April 2025
PUBLISHED 30 April 2025

CITATION
Dang P, Li Z, Zou D, Li H, Cheng Z, Chang L and Lu Y (2025) Monitoring data-driven dynamic safety assessment framework for deep foundation pit construction based on grey clustering and moment method. *Front. Earth Sci.* 13:1583402. doi: 10.3389/feart.2025.1583402

Monitoring data-driven dynamic safety assessment framework for deep foundation pit construction based on grey clustering and moment method

Pengliang Dang[1], Zeliang Li[2]*, Dehai Zou[1], Hangjun Li[1], Zilong Cheng[2], Le Chang[1] and Yadong Lu[1]

[1]Sinohydro Bureau 14 Co., Ltd., Kunming, China, [2]College of Civil and Transportation Engineering, Shenzhen University, Shenzhen, China

To address the safety challenges of deep foundation pit construction under complex conditions, this study proposes a dynamic assessment framework based on grey clustering theory and a moment estimation composite weighting method. A three-level indicator system was constructed, integrating subjective and objective weights through order relationship and entropy weight methods. Grey clustering was employed to classify real-time monitoring data and assess safety levels dynamically. Application to a large-scale water diversion shaft project in Shenzhen verified the model's effectiveness, with assessment results closely matching observed risks during excavation. The framework improves accuracy and responsiveness in uncertain monitoring environments and supports intelligent risk management.

KEYWORDS

deep foundation pit, monitoring data, dynamic safety assessment, grey clustering theory, composite weights

1 Introduction

When there is a need to build underground structures such as shaft foundations, basements, or tunnels, a foundation pit is usually excavated. As urbanization continues to advance and calls for constructing more underground infrastructures, the scale and depth of deep foundation pit engineering are continuously expanding, and their safety issues are receiving increasing attention, especially in densely populated urban areas and karst-prone regions. The pit excavation triggers significant unloading effects and usually negatively disturbs the greenfield ground, which imposes high risks to the surrounding environment and may lead to the disastrous collapse of pit bracing structures and damage to adjacent buildings (Chen et al., 2023). In recent years, multiple foundation pit accidents have occurred, such as the collapse of a metro station project in Hangzhou in 2008 (Gong and Zhang, 2012), the failure of foundation pit support in Nanchang in 2015 (Feng and Lu, 2016), and the pit collapse accident in Nanning in 2019 (Chin et al., 2019), many of which were exacerbated by karst-induced instability (Lv et al., 2020). Causing substantial property losses and casualties. It should be pointed out that these incidents are attributed to unqualified field monitoring or untimely responses to alert monitoring data. Studies emphasize that accurate field monitoring, effective data analysis,

and timely risk management are crucial in preventing foundation pit accidents. For example, numerical analyses have highlighted the importance of understanding the seismic responses of underground structures in complex soil conditions such as liquefiable soils and marine soft soils (Bao et al., 2025), and karst regions (Li et al., 2023). Therefore, performing accurate field monitoring and further effective monitoring data analysis and timely risk management are effective ways to prevent foundation pit accidents. With the advancement of technology, modern deep foundation pit engineering has introduced advanced monitoring techniques and computational models to ensure safety during construction and structural stability. For instance, seismic responses of underground structures in liquefiable soils necessitate precise monitoring and design optimizations to enhance safety during seismic events (Shen et al., 2025; Bao et al., 2024). Similarly, Xu et al. explored the monitoring and assessment methods for ultra-deep diaphragm walls during excavation, providing critical insights into structural stability under high-stress conditions (Xu et al., 2024). In karst regions, unique challenges arise due to hidden cavities, water-filled voids, and unpredictable soil mechanics, which amplify risks of sudden collapses and water inrush during excavation (Xu and Wang, 2022). Recent advancements in machine learning have shown promise in detecting hidden defects in complex geological environments. For example, Bao et al. developed an improved YOLOv8 model with attention mechanisms to detect voids in rebar-affected areas using ground-penetrating radar (GPR) data, demonstrating enhanced accuracy in noisy and cluttered datasets (Bao et al., 2025).

With advancements in monitoring technologies and equipment, effectively utilizing data for risk assessment and prediction has become essential for ensuring safety during deep foundation pit construction. To address this need, several scholars have proposed various methods to predict and assess safety risks throughout the construction process. For instance, Wei et al. introduced a fuzzy analytic hierarchy process (FAHP) combined with evidence reasoning algorithms to evaluate the overall risk level of deep foundation pits, enabling reasonable risk assessments even with insufficient monitoring data (Wei et al., 2020). Similarly, Zhou et al. developed risk prediction models based on support vector machines (SVM) (Zhou et al., 2017) and random forest algorithms (Zhou et al., 2019), both of which have demonstrated reliable validation. Moreover, Wu et al. presented a rapid convergence and high-reliability multi-source data fusion method for assessing subway foundation pit collapse risk, utilizing cloud models (CM) and improved Dempster-Shafer evidence theory to integrate and quickly converge multi-source data under various factors (Wu et al., 2024). Furthermore, Sun applied digital twin technology for real-time risk prediction and control during deep foundation excavation, improving the precision and timeliness of risk management; however, the complexity of the technology and high equipment costs currently hinder large-scale implementation (Sun et al., 2023). Shen established the cloud model theory by using the parameters such as expectation, entropy and super-entropy to represent uncertainty, which provided a new perspective for multi-index comprehensive evaluation (Shen et al., 2025).

With the emergence of an increasing number of safety assessment methods for deep foundation pit construction, the selection of assessment indicators has become more diverse. As a structured framework for assessment methods, assessment indicators directly impact the accuracy and reliability of assessment results. Previous studies have made significant strides in developing safety assessment frameworks for deep foundation pits. However, these methods face notable limitations. FAHP introduces subjectivity due to reliance on expert judgment, whereas SVM struggles with incomplete or uncertain data. Additionally, existing approaches often focus narrowly on structural deformation indicators while neglecting critical factors such as structural internal forces and environmental impacts. This oversight can lead to incomplete risk assessments, particularly in complex geological conditions where multi-factor interactions dominate.

To address the aforementioned issues and provide solutions, this study innovatively proposes a dynamic safety assessment method for deep foundation pit construction based on gray clustering theory and moment estimation composite weights. The innovations of this assessment method include: (1) the introduction of gray clustering theory effectively addresses the uncertainty and incompleteness of monitoring data in practical engineering, enhancing computational efficiency and ensuring the accuracy and timeliness of assessment results; (2) the incorporates monitoring projects from current standards as assessment indicators, eliminating the need for additional resource investment and ensuring the economic viability and applicability of the assessment approach; (3) a multi-layer composite weights approach based on moment estimation is proposed for assigning weights to each assessment indicator, ensuring objectivity and scientific rigor in the distribution of weights.

The rest of this paper is divided into five main sections: Section 2 will elaborate on the theoretical foundations of this research, including the principles of gray clustering theory and moment estimation methods, as well as their application context in safety assessments; Section 3 details the construction process of the assessment model, covering the selection of assessment indicators, the methodology for weight allocation, and the mathematical representation of the model; Section 4 presents the application process and practical effects of the assessment model through specific engineering cases, validating its effectiveness and applicability; Section 5 summarizes the main contributions and practical value of the assessment method, while also discussing the limitations of the study and potential future research directions.

2 Methodology

As a multi-attribute decision-making (MADM) problem (Li et al., 2015), the dynamic safety assessment of deep foundation pit construction needs to consider the interaction between multiple factors, and finally obtain a safety index comprehensively. The assessment of safety indicators requires scientific weight coefficients allocation and reasonable assessment methods to obtain accurately fit actual results.

A scientific and reasonable weight determination method should consider subjective and objective factors. Common subjective weight determination methods include expert evaluation method, analytic hierarchy process (AHP) and order relationship analysis method. The expert evaluation method directly assigns weights to each evaluation indicator through the experience and knowledge of professionals; the AHP quantifies the relative

importance of different factors by constructing a hierarchical model, and determines the weights through a series of comparative judgments; and the order relationship analysis method determines the weights for each indicator by judging the relationship between sequences, which is suitable for situations where clear data is lacking. The calculation of objective weights is usually based on some theoretical methods based on data, among which the entropy weight method is the most universal method. The entropy weight method is based on the objectivity of data and determines the objective weights of each indicator by analyzing the uncertainty of the data. This process is completely based on the inherent characteristics of the data, reducing the possibility of human intervention and errors.

Given the diversity of assessment indicators of deep foundation pit construction and the implicit relationships among them, it is more practical to calculate composite weights by integrating both subjective and objective aspects.

2.1 Weight coefficients

2.1.1 Order relationship analysis method

The Order Relationship Analysis Method (ORAM) is a subjective weight assignment method proposed based on the AHP. This method first qualitatively sorts the indicators and then quantitatively assigns values with comparing adjacent indicators (Ye et al., 2023). After arranging the importance of the assessment indicators in order, the relative importance of other assessment indicators is also uniquely determined, and so are the weights. Compared to the AHP method, when there are many assessment indicators, ORAM does not require a one-time check, solving the problem of inconsistent judgment matrices and greatly improving the computational efficiency of the model. The detailed process of this method include.

Step 1: Determine the order relationship

Establish the set of indicators based on the dynamic safety assessment index system, perform a Delphi method ranking (usually by experts in this area), and ultimately establish a unique order based on importance from the highest to the lowest, as in Equation 1:

$$X_1 > X_2 > \ldots > X_{i-1} > X_i > X_{i+1} > \ldots > X_p \tag{1}$$

Step 2: Calculate the relative importance coefficient

Set Equation 2 as r_I, the ratio of the relative importance of indicator X_{i-1} to X_I and refer to Table 1 for the meaning of r_i:

$$r_i = \frac{x_{i-1}}{x_i} \, (i = 2, 3, \ldots, p) \tag{2}$$

In the formula, *i* represents the relative importance.

Step 3: Weight coefficient calculation

Within the context of sequential relational indicators, designate the weight of the j indicator as w_j' as presented in Equation 3.

$$w_j' = \frac{\alpha_i \prod_{i=j+1}^{p} r_i}{\sum_{k=1}^{p} \alpha_k \prod_{i=k+1}^{p} r_i} \tag{3}$$

TABLE 1 Relative importance of indicators.

r_i	Meanings
1.0	The indicator X_{i-1} is just as important as the indicator X_i
1.2	The indicator X_{i-1} is slightly more important than the indicator X_i
1.4	The indicator X_{i-1} is significantly more important than the indicator X_i
1.6	The indicator X_{i-1} is more important than the indicator X_i
1.8	The indicator X_{i-1} is extremely important than the indicator X_i

Note: 1.1, 1.3, 1.5, and 1.7 respectively indicate importance between neighboring two.

In the formula, α_I is an adjustment factor, which is set in reverse order based on the importance of the indicator.

2.1.2 Entropy weight method

The entropy weight method (EWM) is an important objective weighting method that develops from the concept of entropy, a term mostly used to describe a state of disorder, randomness, or uncertainty. The term is first recognized and used in classical thermodynamics (Akih-Kumgeh, 2016). Generally, the lower the information entropy H_j of an indicator, the greater the variability of its values and the more information it provides. When using the characteristic of entropy to express information quantity, the greater the difference of an indicator among various assessment objects, the greater its role in the comprehensive assessment, and consequently, its weight should also be greater (Wu et al., 2022). As an objective weighting method, EWM calculates weights from the judgment matrix, and it is considered more precise compared to other objective weighting assessment methods (Ahn, 2011). The general process of entropy weight method includes the below key steps:

Step 1: Data standardization.

Formulate the data of each indicator into an i × j judgment matrix, defined as the raw matrix A, and then obtain matrix B through standardization processing Equation 4.

$$b_{ij} = \frac{a_{ij} - \min\left(a_{ij}\right)}{\max\left(a_{ij}\right) - \min\left(a_{ij}\right)} \tag{4}$$

Here, a_{ij} refers to the data in the j row of the i indicator in the judgment matrix, $\max\left(a_{ij}\right)$ is the maximum value of all elements in matrix A, and $\min\left(a_{ij}\right)$ is the minimum value of all elements in matrix A.

Step 2: Proportion of the indicator.

The purpose of proportion is to measure the importance of each assessment objects in that indicator. For standardized data, Equation 5 is used to calculate the proportion of each assessment objects under each index.

$$p_{il} = \frac{b_{ij}}{\sum_{i=1}^{m} b_{ij}} \tag{5}$$

Here, m is the number of assessment objects, pil represents the proportion of the i object in the j index.

Step 3: Calculate the information entropy.

The information entropy for each indicator is calculated utilizing Equation 6.

$$H_j = -k\sum_{i=1}^{m} p_{ij} \ln\left(p_{ij}\right), k = \frac{1}{\ln(m)} \tag{6}$$

Here, k is the normalization coefficient, ensuring that the value of information entropy is between $[0, 1]$. The information entropy reflects the uncertainty of the data. The greater the entropy, the smaller the variability of the data and the lower the differentiation of the index.

Step 5: Calculate objective weights.

Information entropy is introduced into Equation 7 to obtain the objective weight of the index.

$$w_j'' = \frac{1 - H_j}{m - \sum_{j=1}^{m} H_j} \tag{7}$$

2.1.3 Entropy weight method

To balance subjective judgment with objective data in the MADM process, this study employs the moment estimation composite weights method (MECWM) for composite weights, aiming to minimize the influence of subjectivity on the assessment of indicator importance. MECWM is a widely used parameter estimation technique in statistics. This method quantifies the importance of indicators by calculating sample moments and matching them with theoretical population moments (Wooldridge, 2001). This method was first proposed by British statistician Karl Pearson in the late 19th century, estimating the parameters of a probability distribution by matching sample moments with population moments (Pearson, 1936).

In the process of composite weights, MECWM allows us to combine the analysis results of objective data with the subjective judgment of decision-makers. By adjusting parameter estimates to reflect the importance of different indicators, this approach not only enhances the transparency of the decision-making process but also strengthens the reliability of the decision outcomes.

Therefore, this paper will apply MECWM to optimize the combination of weights for the indicators, based on the optimal subjective and objective weight values determined by the ORAM and the EWM, respectively. Employing Equation 8, the composite weights coefficient β_j is ascertained. Thereafter, by integrating the subjective and objective weights into Equation 9, the composite weights w_j for each indicator is ultimately derived. The weight coefficient β_j, determined according to the moment method, primarily reflects the relative importance of subjective and objective factors in decision-making.

$$\beta_j = \frac{w_j'}{w_j' + w_j''} \tag{8}$$

$$w_j = \frac{\beta_j w_j' + \left(1 - \beta_j\right) w_j''}{\sum_{j=1}^{p}\left[\left(1 - \beta_j\right) w_j' + \beta_j w_j''\right]} \tag{9}$$

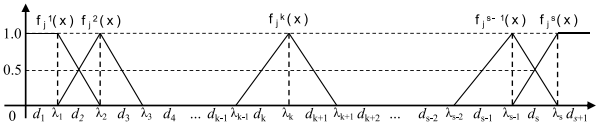

FIGURE 1
Whitening functions of S assessment gray classes.

2.2 Grey clustering theory

The dynamic safety assessment of deep foundation pit construction is a MADM problem. In such scenarios, decision-makers often aim to develop the most reasonable assessment plan in an objective and impartial manner. In deep foundation pit construction, monitoring data often exhibits characteristics such as incompleteness, uncertainty, and variability due to complex geological conditions and construction activities. These uncertainties pose significant challenges in accurately assessing safety risks. Gray clustering theory, based on the whitening weight function of gray numbers, effectively addresses these challenges by integrating the analysis of various indicators to categorize observed objects into predefined classes. It demonstrates good adaptability in addressing multi-attribute decision-making challenges (Li et al., 2015), especially when dealing with uncertain and incomplete data that are common in foundation pit monitoring processes. As an unsupervised learning method, the core idea of gray clustering theory is to effectively manage the grayness of both known and unknown information within a system, thereby revealing the behavioral patterns and intrinsic connections of the system. This method is particularly suitable for situations involving incomplete or highly uncertain information (Li et al., 2015; Liu and Yang, 2017).

Grey clustering theory, rooted in grey system theory, is a powerful tool for addressing uncertainty and incompleteness in data. It operates on the concept of grey numbers' that values with partially known and partially unknown information and employs whitening weight functions to transform ambiguous data into interpretable metrics. The core principle involves dividing data into predefined grey classes' using triangular or trapezoidal membership functions, which inherently accommodate data vagueness. This approach surpasses traditional methods by allowing partial membership in multiple classes, reflecting real-world ambiguities in monitoring data. For example, a displacement value near a safety threshold can be assigned fractional membership to both 'Alert' and 'Warning' classes, capturing transitional states not accounted for in binary systems. This contrasts sharply with binary classification methods, which force data into discrete categories, potentially masking critical transitional risks.

While grey clustering excels in dynamic, uncertain environments, it also outperforms other advanced clustering techniques in critical aspects. k-means clustering, for instance, relies on Euclidean distance and assumes spherical cluster shapes, making it ineffective for non-linear relationships often observed in foundation pit data. Fuzzy C-means introduces

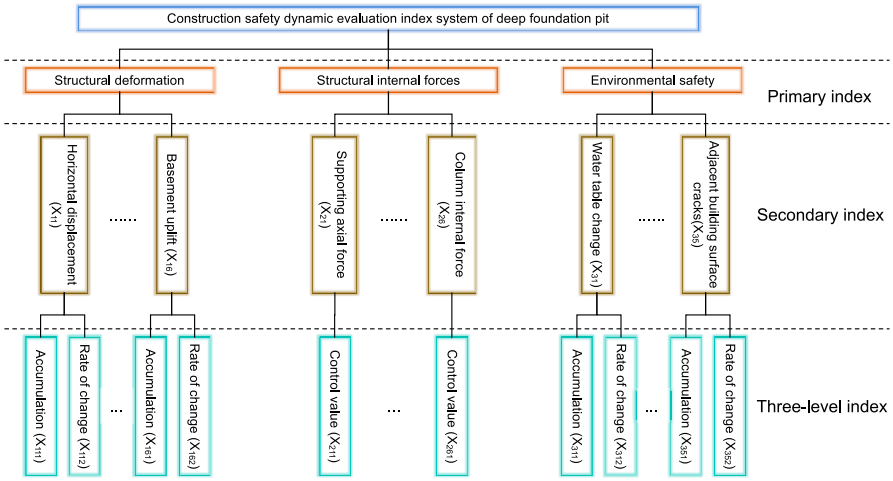

FIGURE 2
The diagram of the dynamic safety assessment index system for deep foundation pit construction.

probabilistic memberships but requires predefined cluster numbers and Gaussian assumptions, which are rarely valid in complex geological settings. Hierarchical clustering lacks scalability for large datasets and is prone to error propagation from early merge decisions, limiting its use in real-time monitoring. In contrast, grey clustering dynamically adapts to data patterns without rigid distribution assumptions, making it uniquely suited for incomplete or evolving datasets typical of deep foundation pit construction.

As a specific application of gray clustering theory, gray clustering analysis primarily includes two types: gray relational clustering and gray whitening weight function clustering (Liu et al., 2017). Gray relational clustering is based on the gray relational matrix, which classifies the observed indicators or objects into predefined categories by calculating the gray relational degree among the assessment objects. In contrast, gray whitening weight function clustering is used to determine whether the observed objects belong to a specific category. This involves establishing a whitening weight function to convert gray data into meaningful whitening values, allowing for appropriate differentiation and processing (Chen et al., 2019). Both the two clustering analysis types offer unique advantages in addressing multi-attribute decision-making problems, particularly in situations with incomplete or highly uncertain information. For the analysis of monitoring data in deep foundation pit construction, the gray whitening weight function clustering method can effectively identify the risks and trends of various factors, particularly in key monitoring indicators such as settlement, displacement, and stress. In contrast, gray correlation clustering focuses more on recognizing the similarities between different data points. Therefore, this study employs the gray whitening weight function clustering method for gray clustering analysis.

Notably, the gray whitening weight function is a piecewise function. Depending on the nature of the observed indicators, different ranges of indicator values correspond to different expressions of the weight function. Let x_{ij} be the observation value of the i assessment object regarding the j indicator (where $i = 1,2,3,\ldots,n$ and $j = 1,2,3,\ldots,p$). $f_i^k(x_{ij})$ denotes the whitening weight function value for the k subclass of the j indicator (where $k = 1,2,3$). According to gray clustering theory, the design of the whitening weight function must meet the following requirements as in Equation 10:

$$\sum_{k=1}^{s} f_i^k(x_{ij}) = 1 \quad \forall x_{ij} \in \otimes \tag{10}$$

Here, $\otimes$ denotes the value range of x_{ij}. The value range of the indicator x_j is divided into S subintervals $[d_1, d_{s+1}]$. The geometric midpoint λ of each subinterval is calculated using the following Equation 11:

$$\lambda_k = \frac{d_{k-1} + d_k}{2} \quad (k \in 1,2,3,\ldots,s) \tag{11}$$

Next, the whitening weight function is constructed as illustrated in Figure 1. Let λ_k represent the whitening weight function value for the k gray class ($k = 2,3,\ldots,s-1$). By connecting point $(\lambda_k, 1)$ with the geometric midpoints λ_{k-1} and λ_{k+1} of the $k-1$ and $k+1$ gray classes, respectively, the triangular whitening weight function $f_i^k(x)$ for indicator X_j concerning the k gray class is obtained, and its expression is given by the following Equation 12:

$$f_j^k(x) = \begin{cases} 0 & x \notin [\lambda_{k-1}, \lambda_{k+1}] \\ \dfrac{x - \lambda_{k-1}}{(\lambda_k - \lambda_{k-1})} & x \in [\lambda_{k-1}, \lambda_k] \\ \dfrac{\lambda_{k+1} - x}{(\lambda_{k+1} - \lambda_k)} & x \in [\lambda_k, \lambda_{k+1}] \end{cases} \tag{12}$$

The triangular whitening weight function for the first gray class is expressed as following Equation 13, the triangular whitening weight function for the s Gy class is expressed as following Equation 14:

$$f_j^k(x) = \begin{cases} 1 & x \in [d_1, d_2] \\ \dfrac{\lambda_2 - x}{\lambda_2 - \lambda_1} & x \in [d_2, \lambda_2] \\ 0 & x \notin [d_1, \lambda_2] \end{cases} \tag{13}$$

10.3389/feart.2025.1583402

TABLE 2 Construction safety dynamic assessment index system of deep foundation pit.

Primary index	Secondary index	Three-level index	unit
Structural deformation (X_1)	Horizontal displacement at the top of bracing and retaining structure (X_{11})	Accumulation (X_{111})	mm
		Rate of change (X_{112})	mm/d
	Vertical displacement at the top of the bracing and retaining structure (X_{12})	Accumulation (X_{121})	mm
		Rate of change (X_{122})	mm/d
	Lateral wall deflection (X_{13})	Accumulation (X_{131})	mm
		Rate of change (X_{132})	mm/d
	Vertical displacement of column (X_{14})	Accumulation (X_{141})	mm
		Rate of change (X_{142})	mm/d
	Vertical surface displacement (X_{15})	Accumulation (X_{151})	mm
		Rate of change (X_{152})	mm/d
	Basement uplift (X_{16})	Accumulation (X_{161})	mm
		Rate of change (X_{162})	mm/d
Structural internal forces (X_2)	Supporting axial force (X_{21})	Control value (X_{211})	kPa
	Axial force of bolt (X_{22})	Control value (X_{221})	kPa
	Earth pressure (X_{23})	Control value (X_{231})	kN
	Pore water pressure (X_{24})	Control value (X_{241})	kN
	Internal Force of Retaining wall (X_{25})	Control value (X_{251})	kPa
	Column internal force (X_{26})	Control value (X_{261})	kPa
Environmental safety (X_3)	Water table change (X_{31})	Accumulation (X_{311})	mm
		Rate of change (X_{312})	mm/d
	Pipeline displacement (X_{32})	Accumulation (X_{321})	mm
		Rate of change (X_{322})	mm/d
	Adjacent building displacement (X_{33})	Accumulation (X_{331})	mm
		Rate of change (X_{332})	mm/d
	Adjacent road settlement (X_{34})	Accumulation (X_{341})	mm
		Rate of change (X_{342})	mm/d
	Adjacent building surface cracks (X_{35})	Accumulation (X_{351})	mm
		Rate of change (X_{352})	mm/d

10.3389/feart.2025.1583402

TABLE 3 Construction safety dynamic assessment index system of deep foundation pit.

Index	Safety level			
	U1	U2	U3	U4
X_{111}	(−∞,10]	(10.20]	(20.30]	(30, +∞)
X_{112}	(−∞,1]	(1,2]	(2,3]	(3, +∞)
X_{121}	(−∞,5]	(5.10]	(10.20]	(20, +∞)
X_{122}	(−∞,1]	(1,2]	(2,3]	(3, +∞)
X_{131}	(−∞,15]	(15.30]	(30.50]	(50, +∞)
X_{132}	(−∞,1]	(1,2]	(2,3]	(3, +∞)
X_{141}	(−∞,10]	(10.20]	(20.30]	(30, +∞)
X_{142}	(−∞,1]	(1,2]	(2,3]	(3, +∞)
X_{151}	(−∞,15]	(15.25]	(25.35]	(35, +∞)
X_{152}	(−∞,1]	(1,2]	(2,3]	(3, +∞)
X_{161}	(−∞,30]	(30.45]	(45.60]	(60, +∞)
X_{162}	(−∞,4]	(4,7]	(7.10]	(10, +∞)
X_{211}	(f_y,60%f_2]	(90%f_y,f_y]∪(60%f_2,70%f_2]	(80%f_y,90f_y]∪(70%f_2,80%f_2]	<80%f_y∪>0%f_2
X_{221}	(f_y,60%f_2]	(90%f_y,f_y]∪(60%f_2,70%f_2]	(80%f_y,90f_y]∪(70%f_2,80%f_2]	<80%f_y∪>0%f_2
X_{231}	(0.60%f_1]	(60%f_1,70%f_1]	(70%f_1,80%f_1]	(80%f_1, +∞)
X_{241}	(0.60%f_1]	(60%f_1,70%f_1]	(70%f_1,80%f_1]	(80%f_1, +∞)
X_{251}	(0.60%f_2]	(60%f_2,70%f_2]	(70%f_2,80%f_2]	(80%f_2, +∞)
X_{261}	(0.60%f_2]	(60%f_2,70%f_2]	(70%f_2,80%f_2]	(80%f_2, +∞)
X_{311}	(01,000]	(1000,1500]	(1,500,2000]	(2000, +∞)
X_{312}	(−∞,400]	(400,450]	(450,500]	(500, +∞)
X_{321}	(−∞,10]	(10.15]	(15.20]	(20, +∞)
X_{322}	(−∞,1]	(1,5]	(1.5,2]	(2, +∞)
X_{331}	(−∞,10]	(10.20]	(20.30]	(30, +∞)
X_{332}	(−∞,1]	(1,2]	(2,3]	(3, +∞)
X_{341}	(−∞,10]	(10.20]	(20.30]	(30, +∞)
X_{342}	(−∞,1]	(1,2]	(2,3]	(3, +∞)
X_{351}	(−∞,10]	(10.13]	(13.15]	(15, +∞)
X_{352}	(−∞,1]	(1,2]	(2,3]	(3, +∞)

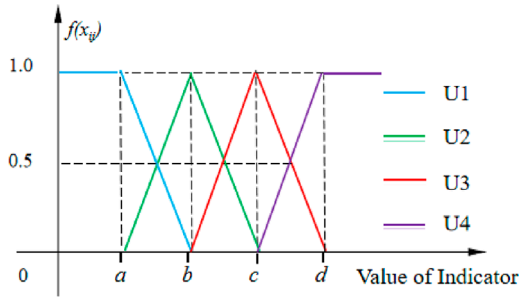

FIGURE 3
Image of whitening weight function of three-level indicators.

$$f_j^k(x) = \begin{cases} 1 & x \in [\lambda_s, d_{s+1}] \\ \dfrac{x - \lambda_{s-1}}{\lambda_s - \lambda_{s-1}} & x \in [\lambda_{s-1}, \lambda_s] \\ 0 & x \notin [\lambda_{s-1}, d_{s+1}] \end{cases} \tag{14}$$

If the weight w_j^k of the k subclass of the j indicator is independent of k (where $w_j^1 = w_j^2 = \ldots = w_j^s$), let σ_i^k denote the gray fixed weight clustering coefficient for the i assessment object in the k subclass. Then as following Equation 15:

$$\sigma_i^k = \sum_{j=1}^{p} f_i^k(x_{ij}) w_j \quad (i = 1, 2, \ldots, m; k = 1, 2, 3) \tag{15}$$

If $\sigma_i^{k^*} = \max(\sigma_i^k) = \max\left[\sum_{j=1}^{p} f_i^k(x_{ij}) w_j\right]$ is satisfied, then the i assessment object belongs to the k^* subclass. Based on Equations 13–15, we can derive the following Equation 16:

$$\sum_{k=1}^{s} \sigma_i^k = 1 \tag{16}$$

This means that the sum of the gray fixed weight clustering coefficients for all subclasses of the i assessment object is equal to 1.

3 Dynamic safety assessment methods for deep foundation pits

3.1 Dynamic safety assessment index system

The selection of proper assessment indicators is a critical aspect determining the effectiveness of the dynamic assessment method of deep foundation pit construction. In this study, the proposed assessment index system is based on the relevant standards (MOHURD, 2019), in order to closely align with actual engineering practices. The selection of assessment indicators must, on one hand consider the complexity of the foundation pit's environment, such as geological conditions, groundwater levels, and the status of surrounding buildings and infrastructure, and on the other hand, carefully weigh the difficulty of data acquisition to ensure the feasibility of equipment deployment and the continuity of data collection. Moreover, the chosen indicators should have a strong ability to reflect the safety status of the foundation pit, capturing changes with adequate sensitivity and accuracy, particularly key indicators like vertical retaining structure deformation and stress or strain responses of the horizontal support structures, which are critical early warning signals of foundation pit instability. Additionally, environmental safety indicators, such as the ground settlement and tilting of nearby structures, should not be overlooked, as they provide insights into the construction's impact on the surrounding environment, allowing decision-makers to intervene in a timely manner (Tan et al., 2023; Zhao et al., 2022). In conclusion, by selecting and designing a rational assessment index system has to incorporate both the bracing structures of pits and also the surrounding influential environment, while balancing the ease of on-site data acquisition (Ye et al., 2021; Qiao et al., 2024).

Based on the classification of deep foundation pit monitoring items, a dynamic safety assessment index system is established to include three primary level indicators and seventeen secondary level process indicators. The three primary level indicators are: structural deformation indicators (X_1), structural internal forces indicators (X_2), and environmental safety indicators (X_3), each incorporates several secondary level indicators, and each secondary level indicator further considers several three-level control indicators. The assessment objectives, assessment criteria, and assessment indicators are at different levels, forming a progressive hierarchical structure. The diagram of the dynamic assessment index system is partially demonstrated here in Figure 2, while the detailed descriptions of indicators are included in Table 2.

3.2 Classification of safety levels

The determination of threshold ranges for the dynamic assessment of deep foundation pit construction safety is based on an analysis of monitoring data from actual projects, combined with references to domestic and international research findings and industry standards (MOHURD, 2019; MOHURD, 2012). The threshold setting also takes into account the specific characteristics of foundation pit projects, including geological conditions, pit excavation depth, retaining structure types, and the complexity of the surrounding environment.

In establishing the threshold ranges for each level, initial reference values were derived from empirical monitoring data on foundation pit deformation, mechanical response of bracing structures, and environmental disturbance monitoring. Significant correlations between foundation pit deformation and instability informed the setting of critical limits for horizontal displacement and vertical settlement of retaining structures such as the diaphragm walls and the sheet pile walls. The mechanical response of support structures during construction also served as a basis for adjusting the alert and warning thresholds for stress-strain indicators of support systems. Additionally, precision of monitoring equipment, dynamic changes during construction, and the influence of the surrounding environment on monitoring data were considered in the threshold determination. For indicators of environment impacts, such as settlement and tilting of adjacent buildings, data from project cases were analyzed to help define appropriate alert and warning thresholds.

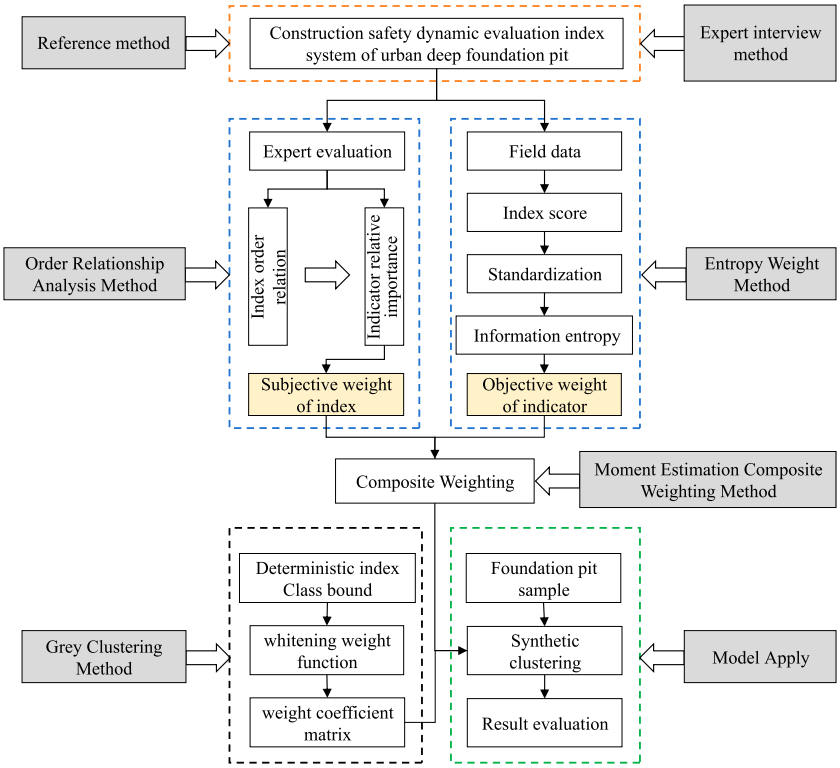

FIGURE 4
Construction dynamic safety assessment model of deep foundation pit.

FIGURE 5
Project routing diagram.

Based on this multi-dimensional analysis, the safety assessment index system U of the deep foundation pit construction is divided into four levels: Safe (U1), Alert (U2), Warning (U3), and Dangerous (U4). Due to space limitations, the final value ranges for each assessment level are detailed in Table 3. According to the divisions of the safety levels, each indicator has three boundary conditions. From these, the four category boundary values (a, b, c, d) can be calculated using Equation 3. Subsequently, combining Equations 4–6, the whitening power functions for each third-level indicator are constructed, resulting in the corresponding weight coefficient matrix. The whitening power functions between different indicators differ only in the category boundary values, with the overall function plots being similar, as shown in Figure 3.

As shown in the figure, the whitening weight function graph of grey clustering theory visually represents how indicator values are mapped to assessment levels, with the horizontal axis denoting indicator values and the vertical axis $f(x_{ij})$ indicating membership weights (0–1). Unlike traditional binary classification methods that impose strict thresholds, this graph inherently reflects the theory's strength in handling uncertainty: adjacent intervals allow partial membership overlaps rather than absolute exclusivity. For instance, an indicator value near threshold b would simultaneously hold fractional membership in both U2 level and U3 level, capturing transitional states typical of incomplete or ambiguous monitoring data. The key points serve as flexible classification boundaries, enabling adaptive quantification of risk levels while accommodating data vagueness. This design ensures the graph provides a robust foundation for the comprehensive evaluation model by translating complex uncertainty into interpretable membership degrees.

3.3 Establishing the dynamic safety assessment model

Based on the determination of the assessment index system and the weight coefficient calculation method, this paper integrates grey

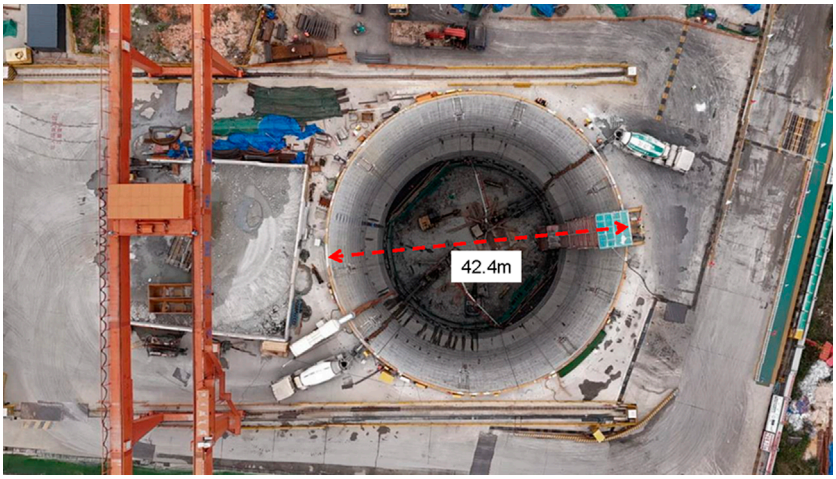

FIGURE 6
Bird-view of the excavated deep shaftLife Science Identifiers.

TABLE 4 Physical and mechanical parameters of soil layer.

Soil layer	$\rho/(g \cdot cm^{-3})$	c/kPa	$\varphi/(°)$	E_e/MPa	v	Thickness/m
Gravel clay	2.66	20	20	12.6	0.35	12
Heavily weathered granite	2.53	350	25	6,200	0.32	21
Rock mass fracture zone	2.58	40	25	2,400	0.32	34
Aeolian granite	2.62	720	25	22,300	0.26	33

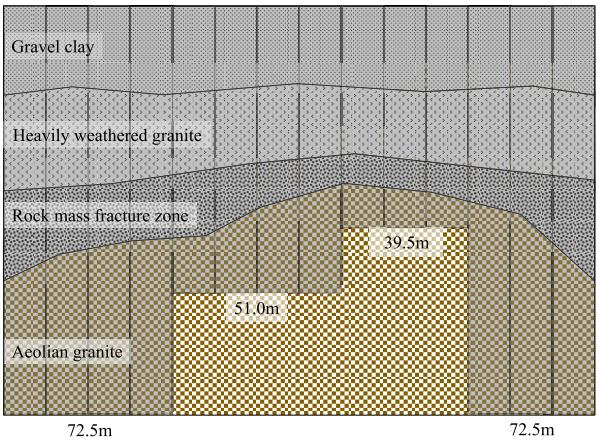

FIGURE 7
Stratum conditions and diaphragm wall layout.

clustering theory to establish a dynamic safety assessment model for deep foundation pit construction as shown in Figure 4. The model combines quantitative and qualitative analyses and relies on real-time monitoring data to dynamically assess the safety status of deep foundation pit construction through grey clustering analysis. It aims to effectively integrate data from multiple sources and expert knowledge, providing a comprehensive dynamic assessment of foundation pit safety through scientific weight allocation and clustering analysis.

The innovative aspect of this model lies in its integration of both quantitative and qualitative analyses, subjective and objective weight allocation, and the application of grey clustering theory to address the complex and variable environment of foundation pit construction and the uncertainty of monitoring data. By leveraging this model, accurate, real-time dynamic assessments of deep foundation pit construction safety can be achieved, providing robust support for risk management and decision-making in the construction process.

Compared to existing methods, our framework offers distinct advantages. Unlike FAHP, which relies on subjective expert judgment, our composite weighting method dynamically balances subjective and objective inputs, enhancing objectivity. In contrast to SVM, which requires large, clean datasets, grey clustering handles incomplete or uncertain data inherent in foundation pit monitoring. Furthermore, our comprehensive three-level index system integrates deformation, internal forces, and environmental factors, addressing the narrow indicator focus of prior studies. These advancements position our framework as a robust tool for real-time, data-driven safety assessment in deep foundation pit construction.

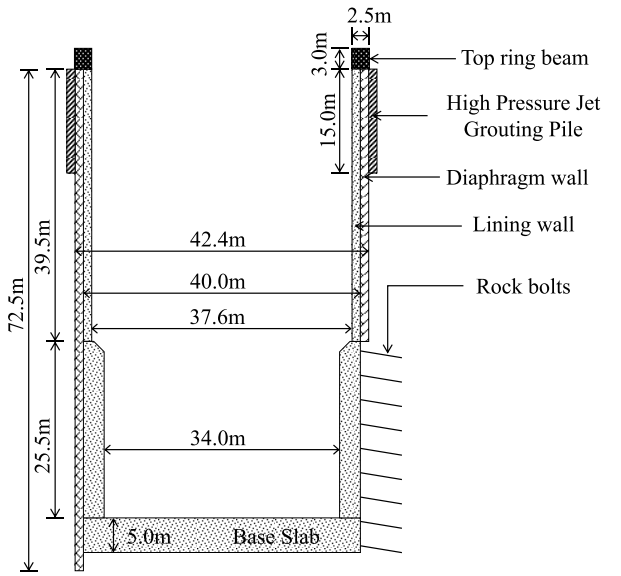

FIGURE 8
Profile of the shaft foundation pit.

To prevent the distortion that a single indicator might cause in the dynamic safety assessment results of the foundation pit, it is necessary to combine the assessment with the prominent primary factor method. Specifically, if any single dynamic monitoring data of the foundation pit exceeds the extreme value of the dangerous situation, the weight of that assessment factor is stipulated to be 1, and the weights of other factors are set to 0. The risk value is then calculated to determine the current danger level of the pit. If none of the deep foundation pit assessment indicators exceed the extreme values of the dangerous situation, proceed to the dynamic safety assessment calculation process. This involves using the assessment index system and the composite weighting values to conduct a dynamic safety assessment calculation for the deep foundation pit construction.

4 Case study

4.1 Project overview

The Luotian-Tiegang Reservoir water diversion tunnel is an important large-scale water conservancy project in Shenzhen (Figure 5), with a designed capacity of 2.6 million cubic meters per day. The main task of the project is to reasonably distribute and use the water from the West River in Shenzhen, optimize the allocation of new foreign water, ensure water supply to the western area of Shenzhen, and meet the long-term urban living and production water needs of Bao'an District and part of Nanshan District. The whole line of the project is located in Bao'an District and Guangming District in the west of Shenzhen, with a total length of 21.68 km and a cross-section diameter of 5.2 m. The main line includes three working diversion shafts, each with an outer diameter exceeding 30 m and a depth of over 60 m.

A dynamic assessment will be conducted on the Wuzhiba diversion shaft, which features the most complex geological conditions. The Wuzhiba diversion shaft is classified as a first-class ultra-deep circular foundation pit, with a final excavation depth of 72.5 m and an internal diameter of 42.4 m (Figure 6).

4.1.1 Geological conditions

The site is located in the western part of Shenzhen, consisting primarily of plain fill, gravelly clay, and granite. The soil profile consists of several distinct layers. Gravel clay at the surface extends to a depth of 12 m, characterized by low density and cohesion which could influence surface stability and water infiltration rates. Heavily weathered granite starts from 12 m down to 33 m, where the rock has degraded substantially, impacting its structural integrity and load-bearing capacity. Between 35.5 and 69.5 m, the fractured rock mass zone contains fragmented rock that could pose challenges for excavation construction. Aeolian granite below 69.5 m is less weathered, offering better stability. Based on the results of exploration and testing, combined with the experience of related local projects, the different mechanical and physical parameters of each soil layer are depicted in Table 4. The geological conditions within the pit area are average, with issues such as low strength, significant variations in weathering, and multiple layers of fractured rock.

4.1.2 Foundation pit excavation and support

In this shaft construction, a 1.2-m-thick diaphragm wall is utilized for retaining structure, but along circumferential direction the wall depths changes with detailed geological conditions, as shown in the layout diagram of the diaphragm wall in Figure 7. The entire diaphragm wall is divided into 30 sections along the circumference. High-pressure jet grouting piles are constructed at the joints of each segment for seepage prevention and reinforcement, with each pile extending 15 m in depth. The shaft will be excavated layer-wises from top to down, and the reinforced concrete shaft walls will be constructed for each newly excavated layer using the bottom-up method. The thickness of the upper part of the lining wall is 1.2 m, which increases to 3 m after reaching the fractured rock layer at a depth of 37.5 m. To ensure the stability and safety of the deep excavation, rock bolts are installed within the fractured rock zones. These bolts, made of HRB400 steel rebar with a diameter of 28mm, are installed at a 15-degree angle to penetrate 6 m depth into the rock, with 2 m spacing in vertical direction. The dimensions of the shaft pit are detailed in Figure 8.

After constructing the diaphragm wall and high-pressure jet grouting piles, excavation of the shaft foundation pit began on 1 May 2023, and the base slab was completed on 24 September 2023, with a total duration of about 147 days. The pit excavation of 75 m deep was divided into 21 layers, with each layer around 3.0 m. Following the excavation of each pit layer, the reinforcement concrete lining was constructed. And the next pit layer excavation was proceeded once the concrete strength (of the previous layer) had reached 80% of the design value, continuing this cycle until reaching the base slab. Specific pit excavation and lining construction parameters are detailed in Table 5.

TABLE 5 Construction parameters at different stages of deep foundation pit.

Stage	Lining Height/m	Lining Thickness/m	Excavation Depth/m
First Layer (Top ring Beam)	3	2.5	3.4
Second Layer	3	1.2	3.9
Third to 13th Layer	3	1.2	3
Fourteenth Layer	3	3	3.3
Fifteenth Layer	2.5	3	2.5
Sixteenth to 20th Layer	3	3	3
Twenty-first Layer	3	3	6.4
Twenty-second Layer (Base Slab)	5	5	

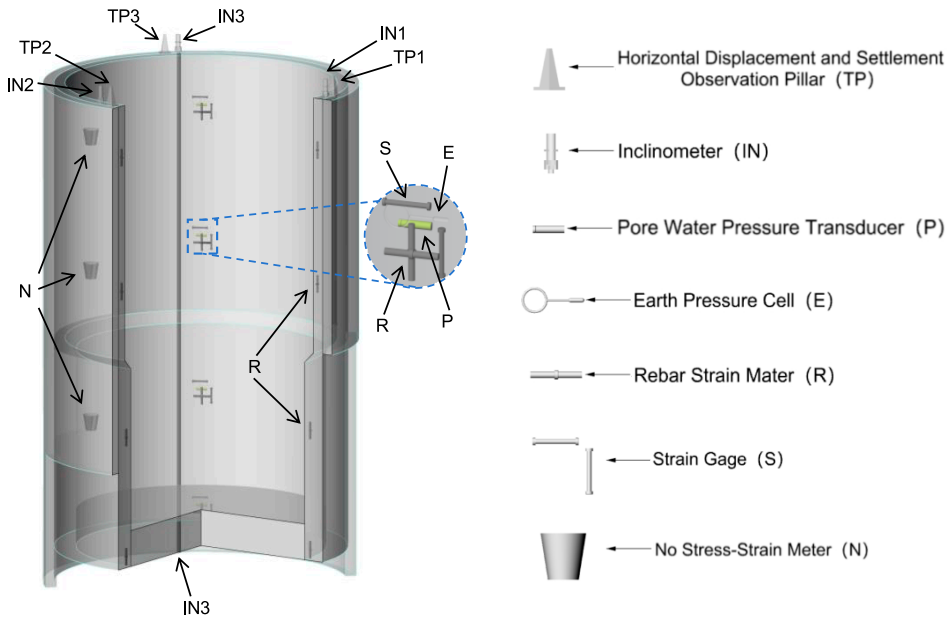

FIGURE 9
Axonometric view of monitoring facilities.

4.1.3 Monitoring plan and data acquisition

To ensure the safety of the deep shaft foundation pit construction, deformation monitoring is conducted simultaneously. Monitoring lines (L1-L3) are laid out at three different depths of the diaphragm wall, as shown in Figures 9, 10. The full monitoring plan is demonstrated in Figure 11 with details described as below.

4.1.3.1 Bracing structural deformation indicators

Three observation piers (TP1~TP3) are set at the top of diaphragm wall to measure the horizontal displacement (X_{11}) and the vertical displacement (X_{12}) at the top of the retaining diaphragm wall. Adjacent to each observation pier, a total of three inclinometer casing (IN1~IN3) is embedded vertically within the diaphragm wall to monitor the lateral wall deflection (X_{13}) during the excavation process. IN1 to IN3 are installed at three different sections of the diaphragm wall, ranging from shortest to longest. For measuring surrounding ground deformation, three monitoring sections are set around the perimeter of the foundation pit, with each section comprising a radial measurement line. Each line has six settlement observation points arranged concentrically from the center of the pit outwards, monitoring the vertical ground displacement (X_{15}). The first observation point is located next to the P1 observation pier, 2 m away from the second point, with subsequent points spaced 8 m apart, totaling 24 observation points (BM1~BM18). Two monitoring holes, each 65 m deep (H1, H2), are set up to monitor the uplift of the shaft pit base (X_{16}). H1 is located near the shaft lining,

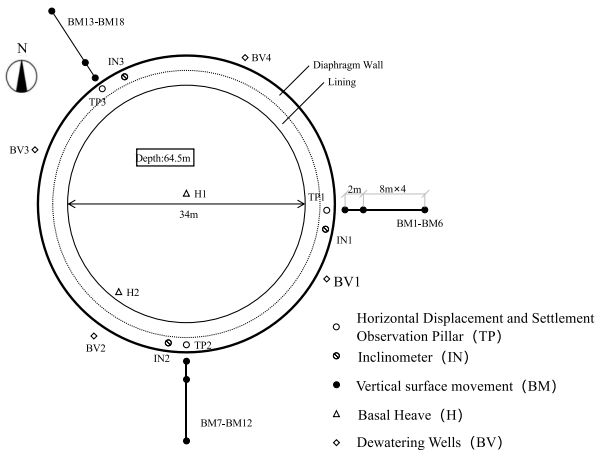

FIGURE 10
Plan view of monitoring facilities.

while H2 is at the center of the shaft. Each hole is equipped with ten magnetic ring-type stratification settlement markers at depths of 10, 18, 26, 34, 40, 46, 52, 56, 60, and 64 m. These rings are removed along with ongoing excavation progresses. Measurements are taken twice at each excavation depth, with one just at completion of layer excavation and the other later just before the subsequent excavation begins.

4.1.3.2 Structural internal forces indicators

Five monitoring sections are set up on the horizontal plane of the foundation pit, with each section having four embedment depths and the base slab. Strain gauges, stress meters, and stress-free meters are installed on the reinforcement bars inside and outside the diaphragm wall, and at the base slab to monitor the supporting axial force (X_{21}), column internal force (X_{26}), anchor axial force (X_{22}), and the internal force of the retaining structure at different depths (X_{25}). Besides, soil and water pressures are measured at designated locations. Four sets of gauges, with each set combining one piezometer and one soil pressure gauge, are installed at four different depths on the outer surface of the diaphragm wall. Two piezometers are placed at the bottom and top of shaft base slab, and two earth pressure gauges are placed at the interface of the shaft base slab and the underlying rock soil to monitor the soil pressure (X_{23}) and pore water pressure (X_{24}) borne by different embedment sections of the diaphragm wall and the base slab.

4.1.3.3 Environmental safety indicators

Groundwater monitoring holes (BV1~BV4) are arranged outside the foundation pit at every 90° to monitor the changes in groundwater level (X_{31}) around the shaft. These holes are drilled and installed outside the settlement observation points, 2.5 m away from them. Additionally, within a 100-m range beyond the edge of the foundation pit, monitoring is conducted for the surrounding environment, including residential houses, roadbeds, pipelines, and other protected facilities along the line. Deformation data is collected for pipeline displacement (X_{32}), adjacent roadbed settlement (X_{34}), adjacent building displacement (X_{33}), and ground surface cracks (X_{35}).

The lateral wall displacements from different excavation stages were collected and demonstrated in Figure 11. In Figure 11A, the shortest segment of the diaphragm wall (IN1) exhibits a gradual increase in lateral wall displacement during various excavation stages. This increase predominantly occurs as the wall traverses vertically through gravel clay and heavily weathered granite layers, which, despite their differing mechanical properties, both possess some degree of flexibility and compressibility, effectively dispersing lateral pressure. However, during the baseplate phase, as the wall transitions from heavily weathered granite to aeolian granite, there is a sudden significant increase in displacement. This surge is due to the high elastic modulus and stiffness of aeolian granite, which causes a drastic change in the properties of the soil layers, concentrating stress in this region, coupled with the maximum vertical pressure induced by increased excavation depth, collectively exacerbating the lateral displacement of the wall at this stage.

In Figure 11B, the medium-length diaphragm wall (IN2) shows a lateral wall deflection curve that transitions gradually from being relatively flat to significantly increasing from the early excavation stage to the baseplate phase. Initially, the displacement is minimal, indicating that the wall is well-supported by the upper soil layers. However, as the excavation depth increases, particularly at the onset of the baseplate phase, there is a noticeable surge in the curve, likely due to construction disturbances such as soil excavation and heavy equipment operation, which dynamically impact the wall in the absence of sufficient lower soil support. This change illustrates that the lateral pressure on the wall increases with excavation depth, directly affecting the stability of the wall due to construction activities.

In Figure 11C, the lateral wall deflection of the longest segment of the diaphragm wall demonstrates a trend of gradual increase with excavation depth, with the most significant displacement occurring during the baseplate phase. Notably, significant displacement anomalies at a depth of 2–5 m are especially prominent, primarily due to the installation of a construction pathway on the lining wall in this region of the diaphragm wall. The establishment and use of the construction pathway led to significant construction disturbances, generating intense vibrations and dynamic loads directly near the retaining structure.

This comprehensive analysis reveals that as excavation depth increases, the displacement of the diaphragm walls gradually increases, especially in areas where soil conditions change or construction activities are concentrated.

4.2 Safety assessment results

4.2.1 Weights of indicators

Ten experts evaluated the primary indices of the deep foundation pit construction safety dynamic assessment system using the Delphi method. The indices were ranked in descending order of importance as structural deformation indicators, structural internal forces indicators, and environmental safety indicators. The relative importance levels between adjacent indicators were set as $r_2 = 1.2$ and $r_3 = 1.3$. Subjective weights for the primary, secondary, and tertiary indices were calculated accordingly, with tertiary indices within the same category assigned equal weight proportions of 0.5.

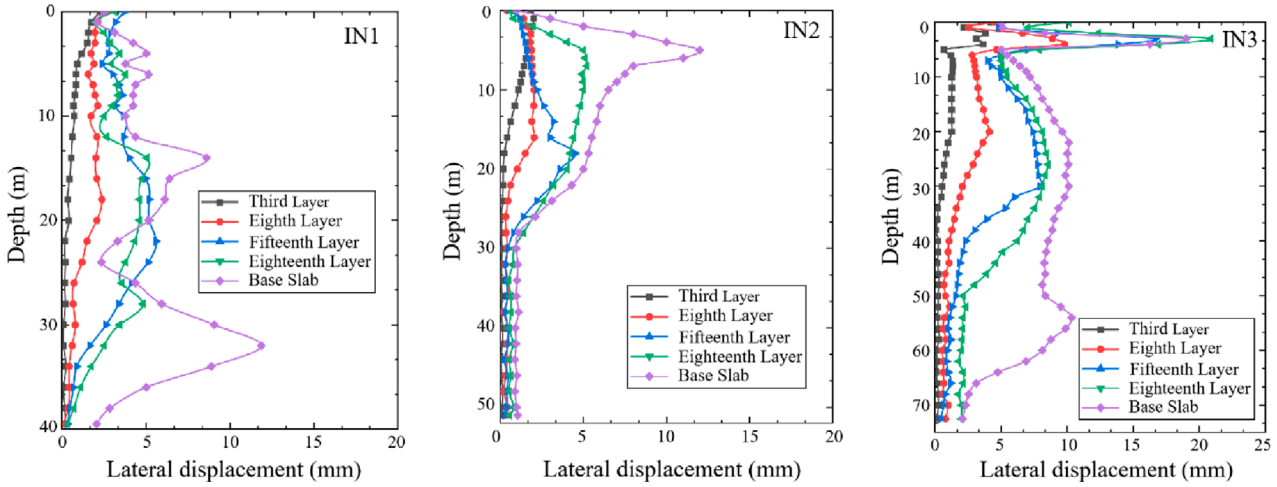

FIGURE 11
Lateral wall deflection at different excavation stages.

Onsite monitoring provided data for the assessment system, which was standardized and used to calculate information entropy and objective weights. Finally, combined weights were determined by integrating subjective and objective weights, and the comprehensive weights of tertiary indicators were calculated. The results are summarized in Table 6.

4.2.2 Dynamic safety assessment

Grey clustering analysis is employed to evaluate the current safety level of the foundation pit construction using real-time monitoring data. An assessment matrix is established based on the on-site monitoring data. By substituting the data of the third-level indicators of the foundation pit into the whitening power functions, the weight coefficient matrix is obtained. Ultimately, the level to which the indicator belongs is determined based on the principle of maximum membership degree, as shown in Appendix. By determining the level through the membership degree, we can clearly observe the varying safety conditions of each monitoring indicator.

Three groups of representative monitoring data were selected respectively, analyzed through the dynamic evaluation of deep foundation pit construction safety, and finally selected the safety data collected during the excavation of the eighth layer, the 15th layer and the Twenty-second Layer. These layers correspond to distinct geological formations and have unique characteristics and risks associated with their excavation. The eighth layer is within the heavily weathered granite, the 15th layer is within the rock mass fracture zone, and the base layer reaches down to the aeolian granite.

The excavation of the eighth layer occurs early in the project timeline, a period when the overall pit stability is comparatively high. This layer consists of heavily weathered granite, which is relatively unstable and prone to crumbling. The weathered nature of the granite increases the risk of sudden soil shifts and collapses. The safety level of foundation pit excavated on the eighth layer is obtained by summarizing the data, as shown in Figure 12. During the excavation of this layer, monitoring focused on structural deformation indicators due to the unstable nature of the soil. The safety indices during this phase showed elevated levels of deformation, indicating stress within the excavation walls.

The eighth layer's elevated deformation risks are directly linked to the geological properties of heavily weathered granite. This layer's low stiffness and high compressibility, combined with the transition from initial diaphragm wall support to permanent concrete lining, created stress concentrations. Monitoring data showed cumulative horizontal displacement of 18 mm and lateral wall deflection of 22 mm. These trends align with the layer's interspersed weathered rock fragments and clay matrix, which reduced load-bearing capacity and amplified deformation under excavation unloading.

The high membership degree value of the top horizontal displacement of the retaining structure (X11) in the safety level U1 indicates that the stability of this indicator is currently good. The membership degree of the deep horizontal displacement (X13) shows that it is mostly in a safe state but with a certain warning trend, suggesting that we need to pay close attention and adjust the support structure in a timely manner. The membership degree analysis of the internal force of the retaining wall (X25) shows that it remains within the safe range in the vast majority of cases, but the membership degree of the warning level should not be ignored, implying that additional monitoring and preventive measures may be needed during the construction process. The high membership degree value of the neighboring building displacement (X33) in U1 provides us with confidence, indicating that the impact of foundation pit construction on the surrounding environment has been effectively controlled.

The 15th layer's fractured rock zone posed significant challenges due to uneven stress distribution and groundwater infiltration. Monitoring data showed a sudden increase in lateral wall deflection, coinciding with the transition to 3 m-thick lining walls. This structural modification altered load transfer mechanisms, reflected in internal force indicators: supporting axial force increased by 25% compared to the previous layer, while earth pressure reached 72% of design capacity. The fractured zone's fragmented rock matrix amplified stress concentrations.

10.3389/feart.2025.1583402

TABLE 6 Comprehensive weight calculation results of indicators at all levels primary index.

Primary index (local weights)	Secondary index (local weights)	Three-level index (comprehensive weight)
Structural deformation (0.438)	X_{11} (0.201)	X_{111} (0.054)
		X_{112} (0.044)
	X_{12} (0.209)	X_{121} (0.028)
		X_{122} (0.020)
	X_{13} (0.256)	X_{131} (0.032)
		X_{132} (0.028)
	X_{14} (0.108)	X_{141} (0.026)
		X_{142} (0.025)
	X_{15} (0.125)	X_{151} (0.026)
		X_{152} (0.024)
	X_{16} (0.131)	X_{161} (0.023)
		X_{162} (0.021)
Structural internal forces (0.342)	X_{21} (0.160)	X_{211} (0.032)
	X_{22} (0.147)	X_{221} (0.029)
	X_{23} (0.226)	X_{231} (0.044)
	X_{24} (0.164)	X_{241} (0.026)
	X_{25} (0.165)	X_{251} (0.021)
	X_{26} (0.109)	X_{261} (0.019)
Environmental safety (0.22)	X_{31} (0.262)	X_{311} (0.023)
		X_{312} (0.021)
	X_{32} (0.226)	X_{321} (0.011)
		X_{322} (0.010)
	X_{33} (0.229)	X_{331} (0.016)
		X_{332} (0.013)
	X_{34} (0.163)	X_{341} (0.008)
		X_{342} (0.006)
	X_{35} (0.140)	X_{351} (0.009)
		X_{352} (0.007)

The 15th Layer Excavation represents a pivotal stage in the construction process, not only because it lies within a fracture zone but also due to changes in the lining wall thickness and construction methodologies. The rock mass fracture zone is characterized by fragmented rock layers with potential voids and uneven stress distribution. This can lead to unpredictable movements and a higher risk of localized failures. The safety level of foundation pit excavated on the 15th layer is obtained by summarizing the data, as shown in Figure 13.

The 20-s layer is also the excavation of the base slab signifies the conclusion of the pit's excavation stages. This final layer provides a comprehensive view of the impacts of construction disturbances

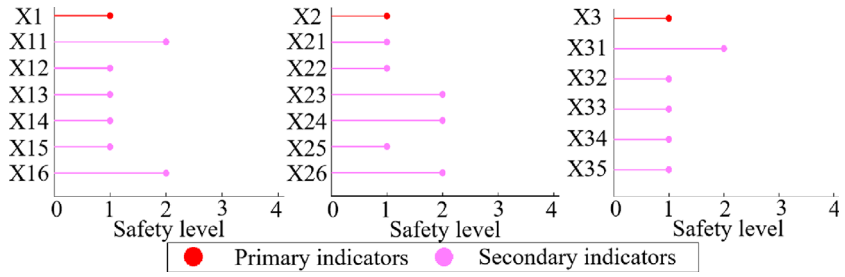

FIGURE 12
Safety dynamic assessment of the eighth layer excavation.

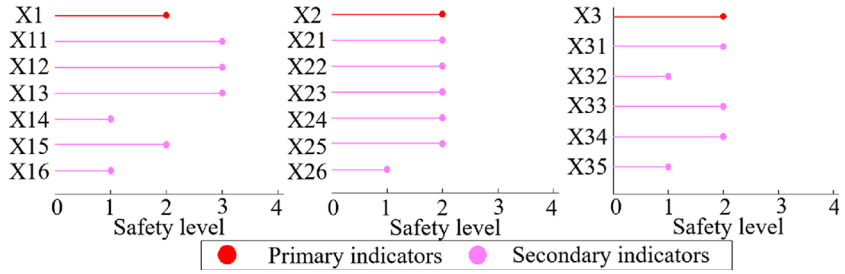

FIGURE 13
Safety dynamic assessment of the 15th layer excavation.

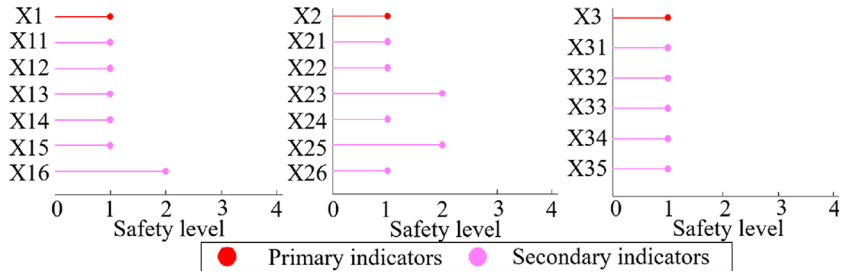

FIGURE 14
Safety dynamic assessment of the base slab excavation.

on the pit's stability throughout the project. By this stage, the data collected offers a complete picture of how well the excavation and support strategies have performed against initial projections and across varying geological conditions. Monitoring at this depth is crucial for ensuring that the base of the pit remains stable and that any signs of undue stress or deformation can be promptly addressed. Finally, the safety level when the excavation of the foundation pit is completed is shown in Figure 14.

4.3 Limitations of this study

In-depth exploration of the effectiveness and application value of the proposed dynamic assessment method for deep foundation pit construction safety, based on gray clustering and moment estimation, leads us to discuss some limitations encountered during the research process. These limitations may include data availability, potential biases in subjective assessments, and the need for further validation in diverse scenarios. Addressing these challenges will be essential for enhancing the robustness and applicability of the proposed methodology.

(1) The safety risk levels established by this research model are based on current regulations used for evaluating deep foundation pit construction safety risks. These regulations often incorporate significant safety margins to ensure absolute project safety, indicating that the assessment method still has room for refinement and enhancement.

Further calibration of the model could provide more precise risk assessments tailored to specific project conditions.

(2) In this study, the construction of the whitening weight function in the application of gray clustering analysis primarily relies on data generated from numerical simulations rather than directly sourced from actual engineering monitoring databases. While numerical simulations provide a relatively controlled and systematic environment for testing and validating the assessment method, they may not fully capture the complexities and uncertainties inherent in real-world construction processes. This limitation suggests the need for further integration of field data to enhance the model's applicability and accuracy.

(3) A notable limitation of this study is the absence of dynamic threshold optimization for monitoring indicators, which could be addressed by integrating data-driven frameworks such as the multi-objective expected value optimization (MEVO) method (Wang et al., 2024). This approach standardizes monitoring data and refines early-warning thresholds through grey relational analysis and Monte Carlo simulations, reducing false alarms and improving risk classification accuracy. For instance, the vertical displacement rate of the retaining structure (X_{112}) could benefit from threshold optimization to better reflect its safety boundaries. Future research should explore this integration to enhance the adaptability of the assessment model under complex geological conditions.

5 Conclusion

This study develops a dynamic safety assessment model for deep foundation pit construction, utilizing a combination of gray clustering and moment estimation weighting. Validation through engineering case studies indicates the model's strong applicability and accuracy. Key findings include.

(1) A comprehensive three-level safety assessment index system comprising 21 indicators is established, incorporating both subjective and objective weight calculations. The gray clustering algorithm categorizes these indicators into structural, mechanical, and environmental safety aspects;

(2) The model's reliability is corroborated by comparisons between numerical simulations and on-site monitoring data from a water diversion well project in Shenzhen, demonstrating consistent trends;

(3) The resilience assessment reveals that the foundation pit is currently at level U1, indicating a safe condition that aligns with actual project observations.

This model provides a scientific basis for optimizing construction strategies and formulating effective risk control measures, highlighting its significant contribution to engineering practices.

The study has confirmed the dynamic assessment method's efficacy for deep foundation pit construction safety and pinpointed areas for future enhancement. Future work should refine safety risk assessment criteria to account for diverse geological and construction factors, promoting more efficient resource use. Additionally, it is essential to gather more real-world engineering data to enhance the accuracy and applicability of the assessment models.

Data availability statement

The original contributions presented in the study are included in the article/supplementary material, further inquiries can be directed to the corresponding authors.

Author contributions

PD: Conceptualization, Methodology, Writing – original draft, Writing – review and editing. ZL: Conceptualization, Investigation, Methodology, Resources, Writing – original draft, Writing – review and editing. DZ: Data curation, Writing – original draft. HL: Data curation, Validation, Writing – original draft. ZC: Investigation, Software, Validation, Writing – original draft. LC: Formal Analysis, Project administration, Writing – original draft. YL: Investigation, Project administration, Writing – original draft.

Funding

The author(s) declare that no financial support was received for the research and/or publication of this article.

Conflict of interest

Authors PD, DZ, HL, LC, and YL were employed by Sinohydro Bureau 14 Co., Ltd.

The remaining authors declare that the research was conducted in the absence of any commercial or financial relationships that could be construed as a potential conflict of interest.

Generative AI statement

The author(s) declare that no Generative AI was used in the creation of this manuscript.

Publisher's note

References

Ahn, B. S. (2011). Compatible weighting method with rank order centroid: maximum entropy ordered weighted averaging approach. *Eur. J. operational Res.* 212 (3), 552–559. doi:10.1016/j.ejor.2011.02.017

Akih-Kumgeh, B. (2016). Toward improved understanding of the physical meaning of entropy in classical thermodynamics. *Entropy* 18 (7), 270. doi:10.3390/e18070270

Bao, X., Huang, J., Shen, J., Wu, X., Wang, T., Chen, X., et al. (2025). A novel method of void detection in rebar-affected areas based on transfer learning and improved YOLOv8. *Tunn. Undergr. Space Technol.* 158, 106440. doi:10.1016/j.tust.2025.106440

Bao, X., Li, J., Shen, J., Chen, X., Zhang, C., and Cui, H. (2025). Comprehensive multivariate joint distribution model for marine soft soil based on the vine copula. *Comput. Geotechnics* 177, 106814. doi:10.1016/j.compgeo.2024.106814

Bao, X., Yuan, H., Shen, J., Liu, C., Chen, X., and Cui, H. (2024). Numerical analysis of seismic response of a circular tunnel-rectangular underpass system in liquefiable soil. *Comput. geotechnics* 174, 106642. doi:10.1016/j.compgeo.2024.106642

Chen, K., Chen, P., Yang, L., and Jin, L. (2019). Grey clustering evaluation based on AHP and interval grey number. *Int. J. Intelligent Comput. Cybern.* 12 (1), 127–137. doi:10.1108/ijicc-04-2018-0045

Chen, X., Shen, J., Bao, X., Wu, X., Tang, W., and Cui, H. (2023). A review of seismic resilience of shield tunnels. *Tunn. Undergr. Space Technol.* 136, 105075. doi:10.1016/j.tust.2023.105075

Chin, Y., Shen, S., Zhou, A., and Chen, J. (2019). Foundation pit collapse on 8 june 2019 in nanning, China: a brief report. *Safety* 5, 68. doi:10.3390/safety5040068

Feng, S. J., and Lu, S. F. (2016). Failure of a retaining structure in a metro station excavation in Nanchang City, China. *J. Perform. Constr. Facil.* 30 (4), 04015097. doi:10.1061/(asce)cf.1943-5509.0000855

Gong, X. N., and Zhang, X. C. (2012). Excavation collapse of Hangzhou subway station in soft clay and numerical investigation based on orthogonal experiment method. *J. Zhejiang Univ. Sci. A* 13 (10), 760–767. doi:10.1631/jzus.a1200120

Li, B., Lin, Z., Chen, Y., Xu, C., Li, P., and Ding, H. (2023). Numerical analysis for supporting and deformation of complex foundation pit groups in unstable areas of karst strata. *Front. Earth Sci.* 11, 1283184. doi:10.3389/feart.2023.1283184

Li, C., Chen, K., and Xiang, X. (2015). An integrated framework for effective safety management evaluation: application of an improved grey clustering measurement. *Expert Syst. Appl.* 42 (13), 5541–5553. doi:10.1016/j.eswa.2015.02.053

Li, D., Liao, F., Wang, L., Lin, J., and Wang, J. (2024). Multi-stage and multi-parameter influence analysis of deep foundation pit excavation on surrounding environment. *Buildings* 14 (1), 297. doi:10.3390/buildings14010297

Li, X., Hipel, K. W., and Dang, Y. (2015). An improved grey relational analysis approach for panel data clustering. *Expert Syst. Appl.* 42 (23), 9105–9116. doi:10.1016/j.eswa.2015.07.066

Liu, S., and Yang, Y. (2017). Explanation of terms of grey clustering evaluation models. *Grey Syst. Theory Appl.* 7 (1), 129–135. doi:10.1108/gs-11-2016-0046

Liu, W., Zhang, J., Jin, M., Liu, S., Chang, X., Xie, N., et al. (2017). Key indices of the remanufacturing industry in China using a combined method of grey incidence analysis and grey clustering. *J. Clean. Prod.* 168, 1348–1357. doi:10.1016/j.jclepro.2017.09.078

Lv, Y., Jiang, Y., Hu, W., Cao, M., and Mao, Y. (2020). A review of the effects of tunnel excavation on the hydrology, ecology, and environment in karst areas: current status, challenges, and perspectives. *J. Hydrology* 586, 124891. doi:10.1016/j.jhydrol.2020.124891

Ministry of Housing and Urban-Rural Development of the People's Republic of China (2019). *Technical code for construction safety of deep building foundation excavations; jgj311-2013*. Beijing, China: China Architecture and Building Press, 4.

Ministry of Housing and Urban-Rural Development of the People's Republic of China (2019). *Technical specification for retaining and protection of building foundation excavations; jgj120-2012*. Beijing, China: China Architecture and Building Press, 6.

Ministry of Housing and Urban-Rural Development of the People's Republic of China (2019). *Technical Standard for Monitoring of building excavation engineering; GB 50497-2019*. Beijing, China: China Plans Publishing House, 34–36.

Pearson, K. (1936). Method of moments and method of maximum likelihood. *Biometrika* 28 (1/2), 34–47. doi:10.1093/biomet/28.1-2.34

Qiao, Y., Xie, F., Bai, Z., Lu, J., and Ding, W. (2024). Deformation characteristics of ultra-deep circular shaft in soft soil: a case study. *Undergr. Space* 16, 239–260. doi:10.1016/j.undsp.2023.09.006

Shen, J., Bao, X., Chen, X., Wu, X., Qiu, T., and Cui, H. (2025). Seismic resilience assessment method for tunnels based on cloud model considering multiple damage evaluation indices. *Tunn. Undergr. Space Technol.* 157, 106360. doi:10.1016/j.tust.2024.106360

Shen, J., Bao, X., Li, J., Chen, X., and Cui, H. (2025). Study on the mechanism of EPWP dissipation at the joints of shield tunnel in liquefiable strata during seismic events. *Soil Dyn. Earthq. Eng.* 188, 109089. doi:10.1016/j.soildyn.2024.109089

Sun, Z., Li, H., Bao, Y., Meng, X., and Zhang, D. (2023). Intelligent risk prognosis and control of foundation pit excavation based on digital twin. *Buildings* 13 (1), 247. doi:10.3390/buildings13010247

Tan, Y., Lu, Y., and Wang, D. (2023). Interactive behaviors of four closely spaced mega excavations in soft clays: case study on an excavation group in Shanghai, China. *Tunn. Undergr. Space Technol.* 138, 105186. doi:10.1016/j.tust.2023.105186

Wang, X., Pan, Y., Li, M., and Chen, J. (2024). A novel data-driven optimization framework for unsupervised and multivariate early-warning threshold modification in risk assessment of deep excavations. *Expert Syst. Appl.* 238, 121872. doi:10.1016/j.eswa.2023.121872

Wei, D., Xu, D., and Zhang, Y. (2020). A fuzzy evidential reasoning-based approach for risk assessment of deep foundation pit. *Tunn. Undergr. Space Technol.* 97, 103232. doi:10.1016/j.tust.2019.103232

Wooldridge, J. M. (2001). Applications of generalized method of moments estimation. *J. Econ. Perspect.* 15 (4), 87–100. doi:10.1257/jep.15.4.87

Wu, B., Zeng, J., Zhu, R., Yang, F., Liu, C., and Xie, Y. (2024). A collapse risk assessment method for subway foundation pit based on cloud model and improved Dempster–Shafer evidence theory. *Sci. Rep.* 14 (1), 2653. doi:10.1038/s41598-024-52643-x

Wu, R. M., Zhang, Z., Yan, W., Fan, J., Gou, J., Liu, B., et al. (2022). A comparative analysis of the principal component analysis and entropy weight methods to establish the indexing measurement. *PloS one* 17 (1), e0262261. doi:10.1371/journal.pone.0262261

Xu, J., and Wang, Y. (2022). Stability analysis and support design methods for rock foundation pit with combination of structural plane and karst cave. *Adv. Civ. Eng.* 2022 (1), 5662079. doi:10.1155/2022/5662079

Xu, Q., Xie, J., Zhu, H., and Lu, L. (2024). Supporting behavior evolution of ultra-deep circular diaphragm walls during excavation: monitoring and assessment methods comparison. *Tunn. Undergr. Space Technol.* 143, 105495. doi:10.1016/j.tust.2023.105495

Ye, F., Sun, J., Wang, Y., Nedjah, N., and Bu, W. (2023). A novel method for the performance evaluation of institutionalized collaborative innovation using an improved G1-CRITIC comprehensive evaluation model. *J. Innovation and Knowl.* 8 (1), 100289. doi:10.1016/j.jik.2022.100289

Ye, S., Zhao, Z., and Wang, D. (2021). Deformation analysis and safety assessment of existing metro tunnels affected by excavation of a foundation pit. *Undergr. Space* 6 (4), 421–431. doi:10.1016/j.undsp.2020.06.002

Zhao, J., Tan, Z., Yu, R., Li, Z., Zhang, X., and Zhu, P. (2022). Deformation responses of the foundation pit construction of the urban metro station: a case study in Xiamen. *Tunn. Undergr. Space Technol.* 128, 104662. doi:10.1016/j.tust.2022.104662

Zhou, Y., Li, S., Zhou, C., and Luo, H. (2019). Intelligent approach based on random forest for safety risk prediction of deep foundation pit in subway stations. *J. Comput. Civ. Eng.* 33 (1), 05018004. doi:10.1061/(asce)cp.1943-5487.0000796

Zhou, Y., Su, W., Ding, L., Luo, H., and Love, P. E. (2017). Predicting safety risks in deep foundation pits in subway infrastructure projects: support vector machine approach. *J. Comput. Civ. Eng.* 31 (5), 04017052. doi:10.1061/(asce)cp.1943-5487.0000700